NanoDome

H2020-NMP-2014-two-stage

NMP-20-2014 Widening materials models

Grant Agreement n. 646121

DELIVERABLE 3.1

Physical-mathematical Description of the NanoDome Mesoscopic Model

WP number: WP3	**Lead Beneficiary: UNIBO**
Type: Report	**Public**
Start of the project: 15/09/2015	**Due date: month 3 (15/12/2015)**

Physical-mathematical Description of the *NanoDome* Mesoscopic Model

Abstract

This document summarizes the physical-mathematical framework of the mesoscopic model for gas phase condensation nanoparticle synthesis to be used within the *NanoDome* project.

Contents

1 Terminology

Nanoparticles are fine particles that falls in a size range smaller than 100 nm [1]. Several different terminology can be found in literature to describe nanoparticle morphology so that the same word (e.g. agglomerate) can have several different meanings [2]. In this physical model nanoparticles will be characterized using the following definitions, based on their morphological properties, according to [1, 3, 4]:

- **Primary particles**: the smallest identifiable individual particles, usually in the size range between 5 and 50 nm and often present as individual crystals ("single crystalline").
- **Agglomerates** ("soft agglomerates"): assemblies of primary particles and/or aggregates loosely held together by weak bonds which may

be due to van der Waals forces or ionic/covalent bonds operating over very small contact areas. Agglomeration is a reversible process. The total surface area is identical with the sum of the surface areas of the individual particles.

- **Aggregates** ("hard agglomerates"): assemblies of partially sintered primary particles held together by strong bonds (covalent/ionic). The surface area of an aggregate is smaller than the sum of all primary particle surface areas. They are usually formed by sintering of agglomerated primary particles.

A TEM image of a typical nanoparticle agglomerate and its idealization as an assembly of primary particles is shown in figure 1.1.

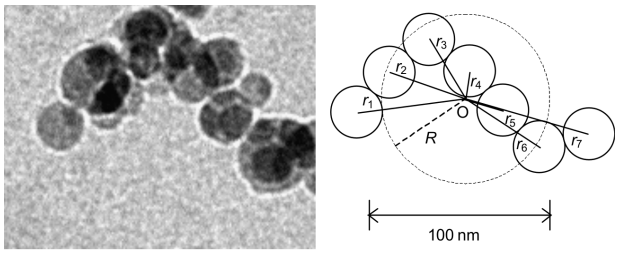

Figure 1.1: TEM image of an actual nanoparticle agglomerate and its simplified representation as an assembly of primary particles. $R = \sum_i m_i r_i^2 / \sum_i m_i$ is the radius of gyration and r_i the distance of the i-th primary particle from the center O of the aggregate mass [1].

With the term **nanoparticle** we will refer to objects that span from a single primary particle (the simplest type of nanoparticle) to complex agglomerates formed by several aggregated primary particles [5]. Examples of nanoparticle morphologies are shown in figure 1.2.

Nanoparticles can be synthesized using several different routes, such as wet synthesis routes, milling techniques and gas-phases synthesis. In this model we focus on **gas-phase condensation** synthesis process (bottom-up approach) in which the thermal decomposition and/or chemical reaction of the precursor results in the formation of a thermodynamically unstable supersaturated vapour followed by spontaneous condensation and nucleation of single vapour atoms to clusters of several molecules [6, 7].

In figure 1.3 the typical gas phase condensation process is represented. Nanoparticles appear by homogeneous nucleation as single primary particles and then coagulate to form agglomerates that can evolve into bigger spherical particles in the extreme case of complete sintering (collision-limited particles) or form aggregates in the extreme case of partial sintering (sintering-limited particles). Heterogeneous nucleation (or surface condensation) that occurs on the surface of primary particles is the other important mechanism of growth that occurs in gas phase condensation synthesis of nanoparticles. In a gas-phase processes, the degree of agglomeration can be tuned by the adjustment of temperature and temperature gradients on the one hand and by the adjustment of pressure and precursor concentration/vapour density on the other hand, having the latter a direct influence on the collision frequency.

2 Atomistic nanoparticle description

In order to clearly identify the quantities to be used in the mesoscopic model and to provide means for the transfer of information between atomistic and mesoscopic models, it is useful to start with a rigorous nanoparticle description at atomistic level and then define by integration the quantities that will be used by the mesoscopic model.

From an atomistic perspective a nanoparticle can be considered as a cluster of several bonded atoms or molecules of different reactive species, each one characterized by a particular spatial position and velocity. Integrations over an atoms subset of the systems forming a nanoparticle can lead to the definition of precise mesoscopic quantities describing the overall nanoparticle status, such as mass, volume, average velocity, center of mass location, moments of inertia and temperature. The evolution in time of this subset can also describe processes like heterogeneous nucleation or surface chemical reactions rates, the interparticle forces and sintering mechanism.

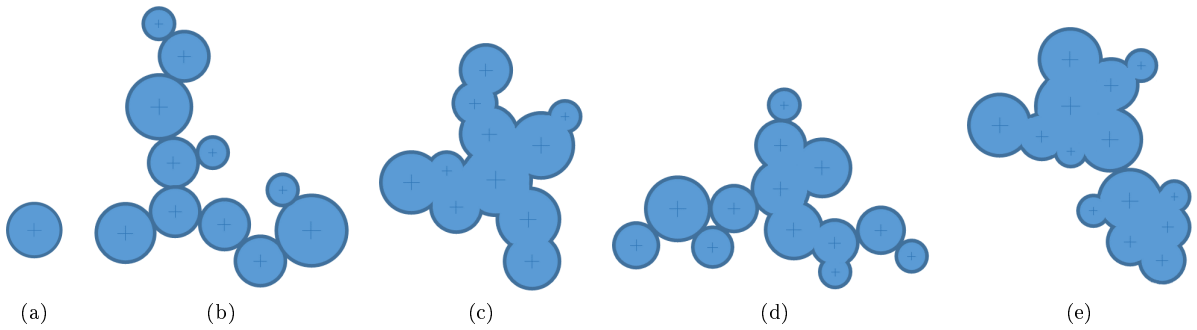

Figure 1.2: Nanoparticle types: single primary (a), agglomerate of primaries (b), aggregate of primaries (c), mixed agglomerates and aggregates (d), agglomerate of two aggregates (e).

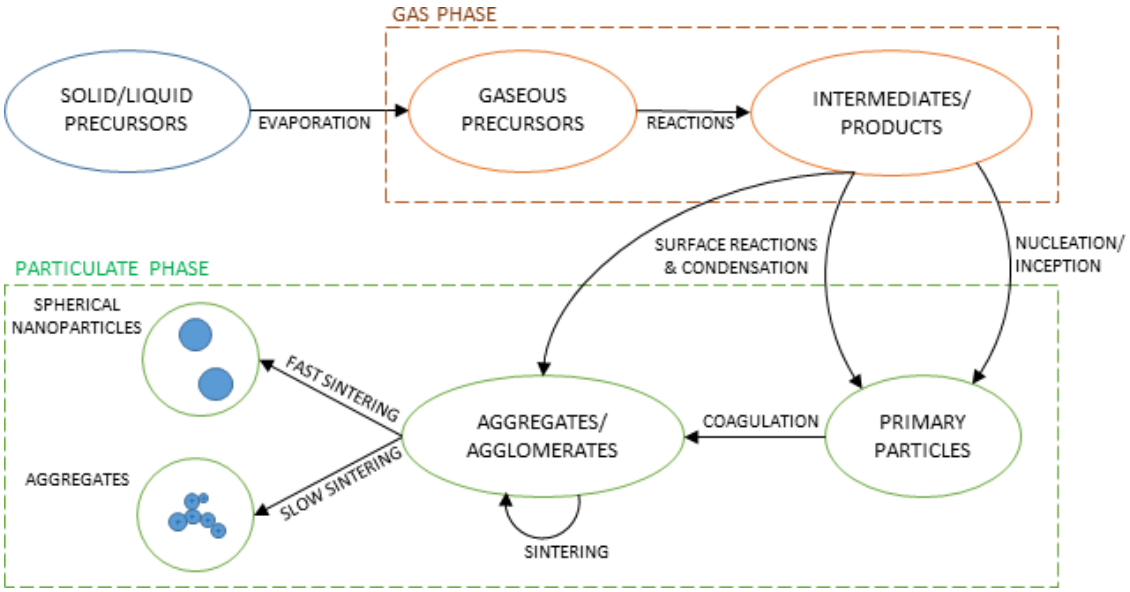

Figure 1.3: Typical gas phase synthesis of nanoparticles by condensation. Spherical particles are obtained in the collision-limited case, while aggregates in the sintering-limited case.

For the purpose of this work the atomic and molecular internal degrees of freedom related to the existence of electronic excited states have been neglected.

In the following sections we will generally refer to **atoms** as the basic objects of the atomistic model, specifying them as **atomic species** or **molecular species** only when needed.

2.1 Molecular dynamics

In the classical molecular dynamics approach an **atomistic system** $\mathcal{A}$ can be defined as a set of **atoms** $a_i(\mathbf{x}_i, \mathbf{v}_i, s_i)$ with $i \in \{1, 2, \ldots, N(\mathcal{A})\}$, where $N(\mathcal{A})$ is the total number of atoms in the system, each one characterized by position $\mathbf{x}_i$, velocity $\mathbf{v}_i$ and species s_i. In this physical model an atomistic system deals with objects can be the defined as atomic species (e.g. $s_i \in \{\mathrm{Ar}, \mathrm{H}, \mathrm{Si}\}$) or molecular species (e.g. $s_i \in \{\mathrm{Al_2O_3}, \mathrm{ZnO}\}$).

The total potential energy U_{tot}^{AT} of the atomistic system $\mathcal{A}$ in its more general form is calculated as

$$U_{tot}^{AT}(\mathcal{A}) = \sum_{i=1}^{N(\mathcal{A})} U_i^{AT}(\{(\mathbf{x}_i, \mathbf{s}_i)\}) \tag{2.1}$$

where $U_i^{AT}(\{(\mathbf{x}_i, \mathbf{s}_i)\})$ is the potential term describing the interaction of the i-th atom with all other particles in the system. In the most general case of a multi-body potential it depends on the position of all atoms in the system $\{\mathbf{x}_i\}$ and on their species type $\{\mathbf{s}_i\}$.

The evolution in time of the system is described by the classical Newton's equation of motion

$$m_i \frac{d^2\mathbf{x}_i}{dt^2} = \mathbf{F}_i \quad i = 1, \ldots, N \tag{2.2}$$

with m_i the mass of the i-th atom species i.e. the s_i-species mass, and

$$\mathbf{F}_i = -\frac{\partial U_{tot}^{AT}(\mathcal{A})}{\partial \mathbf{x}_i} \tag{2.3}$$

is the force acting on the atom a_i.

The classical molecular dynamics approach can be used to predict the evolution of an atomistic system, including nanoparticle formation and evolution in a gas phase environment as shown in figure 2.1.

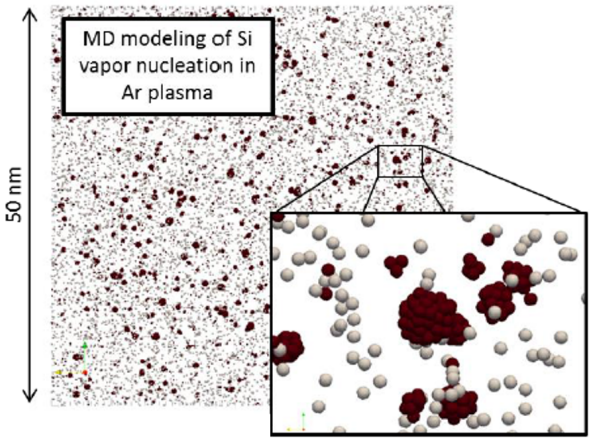

Figure 2.1: Example of nanoparticle formation in a molecular dynamics simulation of a Si/Ar 50%-50% gas mixture with 25000 atoms and Lennard-Jones potential.

2.2 Atomistic definition of a nanoparticle

In order to identify a particular subset of atoms of an atomistic system $\mathcal{A}$ as a nanoparticle some criteria must be introduced. These criteria should also be able to define different non-connected susbsets of atoms each one representing a single nanoparticle. This can be done by checking the connection state of each atom in the system.

2.2.1 Atomic connection criterion

A **connection criterion** $C(a_i, a_j)$ between two atoms in an instantaneous system configuration at time t can be defined requiring that $r_{ij} \leq r_0$, where r_{ij} is the interatomic distance between a_i and a_j and r_0 a characteristic connection distance chosen according to the interatomic potential of each particular species. This simple criterion is very easy to implement and it is commonly used in Molecular Dynamics.

2.2.2 Nanoparticle definition

According to a chosen connection criterion $C(a_i, a_j)$ it is possible to propose the following definitions:

- A **dimer** is an atoms pair (a_i, a_j) with $a_i, a_j \in \mathcal{A}$ that satisfies a chosen bonding criterion $C(a_i, a_j)$.

- A **nanoparticle** is a subsystem NP of an atomistic system $\mathcal{A}$ consisting of $N(NP)$ atoms, with $N(NP) \leq N(\mathcal{A})$, so that $\forall a_l, a_m \in NP$ a connection between the two a_l, a_m atoms can be found, traveling through dimers.

For two single nanoparticles NP_i and NP_j the relation $NP_i \cap NP_j = \emptyset$ must hold.

This definition can cover all possible nanoparticle types shown in figure 1.2, from a single primary particle to complex agglomerates of aggregates, if the $C(a_i, a_j)$ criterion is defined using a sufficiently general interatomic potential covering agglomeration and sintering mechanisms.

In case of atoms defined as atomic reactive species, an intermediate step for the identification of monomers should be included in the definition, together with a connection criteria based on the monomers interaction potential.

2.2.3 Nanoparticle properties

Properties of a NP nanoparticle can be easily defined by integration of atomistic quantities in the subset $NP \subset \mathcal{A}$. For example, nanoparticle mass $m(NP)$, center of mass $\mathbf{x}_{cm}(NP)$ and average velocity $\mathbf{u}(NP)$ can be defined as

$$m(NP) = \sum_{i=1}^{N(NP)} m_i \tag{2.4}$$

$$\mathbf{x}_{cm}(NP) = \frac{\sum_{i=1}^{N(NP)} m_i x_i}{m(NP)} \tag{2.5}$$

$$\mathbf{u}(NP) = \frac{\sum_{i=1}^{N(NP)} m_i \mathbf{v}_i}{m(NP)} \tag{2.6}$$

Average temperature of the nanoparticle NP can be defined as

$$T(NP) = \frac{\sum_{i=1}^{N(NP)} m_i v_i^2}{3k_B N(NP)} \tag{2.7}$$

assuming that $|\mathbf{u}(NP)| \ll |\mathbf{C}_i|$, so that $\mathbf{v}_i = \mathbf{u}(NP_i) + \mathbf{C}_i \cong \mathbf{C}_i$, where $\mathbf{C}_i$ is the peculiar velocity of the i-th atom. This is equivalent to assume that the kinetic energy of the nanoparticle is negligible with respect to its thermal energy.

The population $\eta_s$of a particular species s in a nanoparticle NP can be calculated by a simple summation on all $a_i \in NP$ for which $s_i = s$.

Finally, knowing the spatial distribution of each atom also the calculation for the moment of inertia of the nanoparticle is straightforward.

2.3 Atomistic description of nanoparticle synthesis mechanisms

According to the previous definitions, the atomistic system $\mathcal{A}$ in a classical molecular dynamics simulation can be unequivocally partitioned at each time step in several subsets:

- nanoparticles (multiple subsets, not mutually connected)

- non-bonded atoms (single subset representing the gas phase)

Analyzing the evolution in time of each of these subsets it is possible to evaluate the quantities referring to the mesoscopic nanoparticle system and to the evolution of the gas phase.

2.3.1 Nucleation

Homogeneous nucleation rate can be calculated by counting the appearance of new nanoparticles subsets NP_i in time, while heterogeneous nucleation rate (surface condensation) by monitoring in time the growing rate of NP_i. The rate of heterogeneous nucleation of species s for a nanoparticle $NP_i$is:

$$F_s(NP_i) = \frac{\eta_{i,s}(t + dt) - \eta_{i,s}(t)}{dt}$$

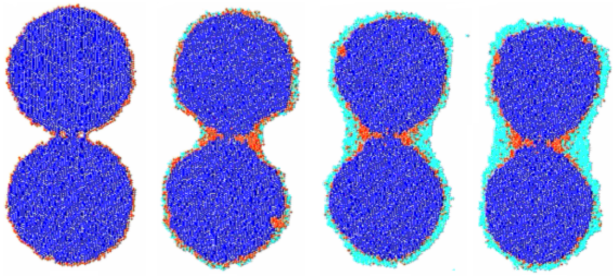

Figure 2.2: Sintering of two equally sized nanoparticles at successive time steps. Bulk, surface and heterogeneous nucleated atoms are coloured in blue, red and cyan respectively [8].

Each nucleation event leads to the reduction of the gas phase atomic population.

2.3.2 Coagulation and sintering

Coagulation occurs as soon as two atoms each one belonging to a different nanoparticle NP_i and NP_j start to be connected, satisfying the C criterion. The coagulation event leads to the formation of an agglomerate between nanoparticles and to the formation of a new nanoparticle $NP_i \cup NP_j$. Depending on the temperature and material properties, the agglomerated particles may sinter to form an aggregate. The sintering process can be described by monitoring the evolution in time of the distance between center of mass of the previously unconnected nanoparticles atoms subsets.

Heterogeneous nucleation may increase the size of the aggregate during sintering process. An example of molecular dynamics sintering prediction can be found in [8], for simple 2D Lennard-Jones bounded atoms.

2.3.3 Diffusion of reactive species

In case of reactive species, the surface reactions between species (e.g. Si/H) may lead to a **radially dependent composition** of the nanoparticle. The radial composition of a primary particle (that can be assumed to be of spherical shape) can be measured by using a radial distribution function $g(r)$ that describes the probability to find a particles of species s_j with distance r from the center of mass of the primary particle. For its computation one determines the number of s_j particles in the shell between r and $r + \delta r$ and divide for $4\pi[(r + \delta r)^3 - r^3]/3$.

3 Mesoscopic model definition

The mesoscopic model is a **coarse grained molecular dynamics** model focused on nanoparticles. Nanoparticle formation is described by classical nucleation theory while nanoparticle dynamics together with the mechanisms of sintering and chemical reactions kinetic are modelled and solved for the prediction of aggregates and agglomerates formation and morphology.

3.1 Model scope and terminology

The mesoscopic model covers:

- **nanoparticle size** from 10 to 200 nm
- a **volume domain** with characteristic length from 1 to 10 μm
- an estimated **number of nanoparticles** in the domain from 100 to 100,000
- a simulation **time scale** from 1 up to 100 ms.

In order to distinguish the entities with respect to the atomistic model, in this section we will refer with the term **molecule** to the atomic compounds that are present in the gas phase and that can constitute a nanoparticle or interact with its surface. Molecules can be atomic species (e.g. Ar, Si, H) or molecular species (e.g. Si-H,Si-N, Si-O, ZnO). [1]

The basic discrete physical object of the mesoscopic model (a.k.a. grain, pseudoatom) is the **minimum thermodynamically stable cluster** of molecules that is called **primary particle**. Since free molecules are smaller than a primary particle, they

[1] It is of paramount importance to define the molecule species that are present only in the gas-phase, the surface reacting species, the condensing species and the species present only in the condensed-phase.

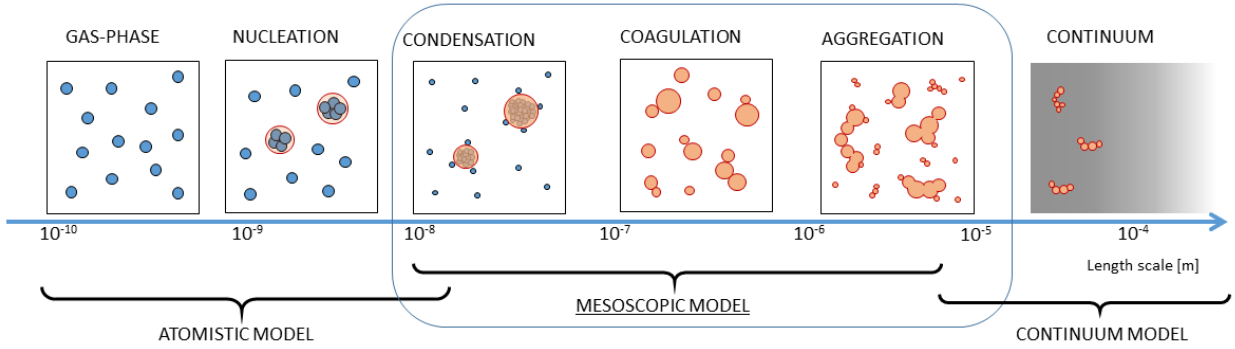

Figure 3.1: Mesoscopic model scale range.

are not included the model as distinct discrete objects; instead they are described using integral thermodynamic quantities (i.e. temperature, species density) and will be addressed in the following section as the gas phase.

The effect of the presence of a free molecules gas phase on nanoparticle formation and growth is taken into account using material laws that describe its effect on the mesoscopic entities (i.e. heating, brownian motion, nucleation, thermodynamics). Primary particles appear by homogeneous nucleation and grow by heterogenous nucleation depending on the gas phase properties and according to nucleation theory predicted rates.

More complex physical objects considered in the models are agglomerates and aggregates of the basic object, the primary particles. Their evolution is predicted until the end of the synthesis process, typically after some tens of ms, when they reach a size around 100 nm.

3.2 Definition of the mesoscopic system

The **mesoscopic** system $\mathcal{MS}$ can be defined as a set of **particles** p_i with $i \in \{1, 2, \ldots, N(\mathcal{MS})\}$ where $N(\mathcal{MS})$ is the number of particles in the system, and a free molecules **gas phase** $\mathcal{GP}$ characterized by its thermodynamic properties. The **particles** p_j constitute the basic objects of the mesoscopic model.

A **nanoparticle** NP is a collection of $N(NP)$ particles $\{p_i\} \subset \mathcal{MS}$ connected together by weak bonds due to interparticle potential (agglomerate) or hard bonds by sintering (aggregate) and a list of connections $\{C_{ij}\}$ between particles storing the information about connection type and sintering evolution.

The simplest nanoparticle is composed by a single particle so that a new nanoparticle is created when a particle is formed by nucleation. For two different nanoparticles the relation $NP_i \cap NP_j = \emptyset$ holds.

An **aggregate** AG is the subset of $N(AG)$ particles inside a nanoparticle $\{p_j\} \subset NP$ that are connected together by sintering. While agglomeration is a reversible process, sintering is non reversible. The relations $AG_i \subset NP$ and $AG_i \cap AG_j = \emptyset$ always holds.

These concepts will be defined in detail in the next sections.

3.3 Gas phase

The gas phase $\mathcal{GP}$ is constituted by **free molecules and atoms** which are below the mesoscopic model length scale (minimum stable cluster diameter) and it is characterized by time dependent **thermodynamic scalar quantities** such as: temperature $T(t)$, pressure $p(t)$, the total number of molecules N_{gas} and species molar concentration $C_s(t)$, with $s \in [1, \ldots, S]$, being S the total number of species in the system. A species can be an atomic species (e.g. Ar, Si) or a molecular species (e.g. Si-H,Si-N, Si-O, ZnO).

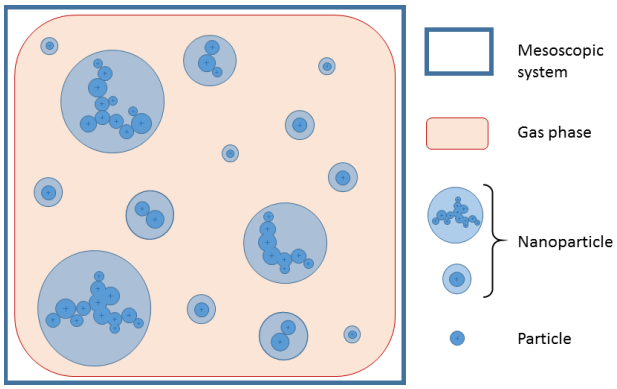

Figure 3.2: Conceptual scheme of the mesoscopic model and its subsets.

In case of **coupling with a continuum** model all these quantities are given as boundary conditions, coming from the solution of the fluid dynamics equations including diffusion and reactions of species at reactor scale. Turbulence effects on transport phenomena and chemical reaction rates are taken into account at continuum scale and then transferred to mesoscopic scale by means on turbulence micromixing models.

If the mesoscopic domain is considered as an **isolated system (0D reactor)**, the chemical species concentration is calculated according to the possible reactions between species and their interactions with particles using non-equilibrium or equilibrium chemistry.

3.3.1 Turbulent mixing

The turbulent micromixing phenomenon can be simulated using a variety of models presented in the literature.

The two most common models include the **Interaction by Exchange with the Mean (IEM)** mixing model and the **coalescence-dispersion (Curl)** mixing model.

The **IEM** (also known as the linear mean square estimation or LMSE) mixing model is a deterministic model in which all scalars relax to a mean value via an exponential decay process [9]. The main features of the model are its simplicity and low computational effort.

For a single scalar the IEM model is given by

$$\frac{d\psi(t)}{dt} = -\frac{1}{\tau_m}\left(\psi(t) - \langle\phi\rangle\right) \tag{3.1}$$

where $\langle\phi\rangle$ is the Favre averaged mean.

The **coalescence-dispersion** mixing model was first proposed by Curl and provides a phenomenological model of turbolent mixing [10]. The model randomly (using a uniform distribution) select pairs (denoted with p and q) of particles and fully mixes them, such that each particle assumes the mean composition of the particle pair

$$\begin{aligned}\phi^{(p,new)} &= \phi^{(p)} + \frac{1}{2}a(\phi^{(q)} - \phi^{(p)}) \\ \phi^{(q,new)} &= \phi^{(q)} + \frac{1}{2}a(\phi^{(p)} - \phi^{(q)})\end{aligned} \tag{3.2}$$

where a is uniformly distributed between [0,1].

The mixing models are parameterised by a scalar mixing rate, defined in terms of a mixing time

$$\frac{1}{\tau_m} = \frac{C_\phi}{2\tau} \tag{3.3}$$

where τ_m is a turbulence timescale and C_Φ is a mechanical-to-scalar timescale ratio. The value of C_Φ is specified as a user-defined input.

The turbulence timescale τ is defined in terms of turbulent kinetic energy k and energy dissipation ϵ

$$\tau \approx \frac{k}{\epsilon} \tag{3.4}$$

3.3.2 Turbulence length scale

It is reasonable to assume that turbulence can affect directly the various synthesis processes only when the **dimension of eddies is smaller than the characteristic size of the process**; this hypothesis is grounded on the idea that all particles located in the same eddy are affected in the same way, leaving the various interaction processes between them unmodified. Thus, the relative diffusion of two colliding elements is modified only if their distance is larger than the surrounding eddy. In order to compare the characteristic process length with the dimension of eddies,

Kolmogorov's length scale μ is used as a parameter, defined as

$$\mu = \left(\frac{\nu^3}{\epsilon}\right)^{1/4} \tag{3.5}$$

where ν is the kinetic viscosity and ϵ the energy dissipation.

As shown in [11], for an ICPT plasma reactor the characteristic length of eddies is much larger than the expected nano-powders in the whole reaction chamber. This means that for this particular reactor particles interacting with other particles or with vapour monomers are all subjected to the same turbulent eddy.

When this condition holds, turbulence effects on particle/particle interactions should be neglected, retaining its effect only for what concerns the fluctuations of the gas phase quantities.

3.3.3 Non-equilibrium chemical kinetics

Following [12] the evolution of the chemical species in time is determined by the chemical kinetics conservation equations together with Dalton's law applied to all the I possible reversible reactions involving N_g chemical species that can take place in the gas phase. The reversible reactions can be written in general form

$$\sum_{k=1}^{N_g} \nu_{ki}^{'} \chi_k \rightleftharpoons \sum_{k=1}^{N_g} \nu_{ki}^{''} \chi_k \tag{3.6}$$

where $\nu_{ki} = \nu_{ki}^{''} - \nu_{ki}^{'}$ are the forward and reverse stoichiometric coefficients of the k species of the i reaction, with $i \in \{1, \ldots, I\}$, and $\chi_k$the chemical symbol for the k species.

$$\frac{dC_s}{dt} = \dot{m}_s(C_s, T) + \dot{g}_s(\mathcal{MS}) \tag{3.7}$$

$$p = N_{gas} \sum_{s=1}^{S} C_s k_B T \tag{3.8}$$

for $s = 1, \ldots, S-1$, where $\dot{m}_s$ is the rate of production of species s computed using Arrhenius expressions and g_s is the source term that takes into account nucleation (heterogeneous and homogeneous) and reactions on the nanoparticles surface. These terms are calculated as

$$\dot{m}_s = \sum_{i=1}^{I} \nu_{si} q_i \tag{3.9}$$

$$q_i = k_{f_i} \prod_{k=1}^{N_g} [C_k]^{\nu_{ki}^{'}} - k_{r_i} \prod_{k=1}^{N_g} [C_k]^{\nu_{ki}^{''}} \tag{3.10}$$

with $k_{f_i} = A_i T^{\beta_i} \exp(-E_i/RT)$ and $k_{r_i} = k_{f_i}/K_i$ where A_i,β_i and E_i are given as input and K_i calculated by thermochemical data.

3.3.4 Equilibrium composition

Under equilibrium composition assumption the model can be simplified and the species concentration can be calculated at each timestep taking into account species disappearance by nucleation (heterogeneous and homogeneous) and reactions on the nanoparticles surface.

Given the total amount of species in the volume, the composition can be calculated using the classical approach of **minimizing the Gibbs free energy**. Since this a very well known method we refer to literature for its description and to [13] for details on a robust solution algorithms for its implementation.

3.4 Particle

The basic object of the mesoscopic model is a **particle**, that overlaps with the concept of primary particle at the beginning of its life, but can substantially evolve growing by coagulation and heterogeneous nucleation and changing its chemical composition by surface reactions and chemical kinetics of the condensed species.

3.4.1 Definition

A **particle** $p_i(\mathbf{x}_i, \mathbf{v}_i, \{\eta_s\})$ is a collection of $N(p_i)$ molecules and is characterized by its position $\mathbf{x}_i$, velocity $\mathbf{v}_i$ and the composition in terms of number of each contained species $\{\eta_s\} = \{\eta_1, \eta_2, \ldots \eta_S\}$, with S

the number of molecular species in the system. Particles are assumend to be of **spherical shape**. From these definitions follows that

$$N(p_i) = \sum_{s=1}^{S} \eta_s \tag{3.11}$$

Particle mass $m(p_i)$ is defined as

$$m(p_i) = \sum_{s=1}^{S} m_s \eta_s \tag{3.12}$$

while particle volume $v(p_i)$ is derived by

$$v(p_i) = \frac{m(p_i)}{\rho(p_i)} \tag{3.13}$$

with $\rho(p_i)$ the bulk density of the material obtained by averaging the bulk densities ρ_s of the S molecular species in the system using η_s as weights. Bulk densities should refer to solid or liquid state, and to particular phases, depending on the temperature[2].

Particle radius is calculated as

$$r(p_i) = \left(\frac{3v(p_i)}{4\pi} \right)^{\frac{1}{3}} \tag{3.14}$$

In case of radially dependent composition the function $\tilde{\eta}_s(r)$ can be defined, satisfying

$$\eta_s = \int_0^{r(p_i)} \tilde{\eta}_s(r) \tag{3.15}$$

The center of the particle is located at its center of mass $\mathbf{x}_{i,cm}$, as defined in equation (2.5) for an atomistic system. Similarly the velocity $\mathbf{v}_i$ coincides with $\mathbf{u}(NP)$ of 2.6.

Particle shape is assumed to be spherical so that its **tensor of inertia** can be approximated as

$$I = \begin{bmatrix} \frac{2}{5} m_i (p_i)^2 & 0 & 0 \\ 0 & \frac{2}{5} m_i r(p_i)^2 & 0 \\ 0 & 0 & \frac{2}{5} m_i r(p_i)^2 \end{bmatrix}$$

[2]Size-dependent melting temperature will be considered, according to literature available data on each particular material.

Since particles with a small number of molecules may show a non-spherical arrangement this assumption is completely valid only for sufficiently large particles. For Si the crystalline structures starts to produce almost spherical clusters with $n \gtrapprox 30$.

Particles can be defined from molecular dynamics simulation as shown in 2.2.2. In this model the reduction from atomistic to mesoscopic description is applied only to nanoparticles made of a single primary, between homogeneous nucleation and coagulation phases. Reduction from atomistic description can be done by using a **mapping matrix** from the set of atomic coordinates to a unique nanoparticle configuration in the mesoscopic system

$$\mathbf{x}_{meso} = \mathbf{M}_{\mathbf{x}} \mathbf{x}_{atom}$$

where $\mathbf{x}_{meso}$ is the collection of all N_{meso} particles coordinates, $\mathbf{x}_{atom}$ the collection of all N_{atom} molecules coordinates and $\mathbf{M}_{\mathbf{x}}$ the $3N_{meso} \times 3N_{atom}$ mapping matrix (equivalent to centers of mass calculation). A similar approach can be used for the reduction of the velocities from the atomistic to mesoscopic description introducing a $\mathbf{M}_{\mathbf{v}}$ mapping.

The reduction of a particle from a cluster of atoms to a simple 0D geometric point leads to **loss of information** about its internal degrees of freedom, in particular regarding:

- the dissipation phenomena occurring inside the real particle
- the possibility for a particle to rotate around an arbitrary axis
- the possibility to oscillate around the shape of minimum surface tension energy (spherical shape)

While these phenomena can affect e.g. the way particles coagulate or the mechanisms of energy transfer, their influence on the model prediction is assumed to be negligible.

3.4.2 Formation

Particles appear in the computational domain as primary particles with **random positions and velocity** (avoiding overlapping with other entities),

in thermal equilibrium with the gas phase system $T(p_i) = T$ and with a production rate and initial size determined by Classical Nucleation Theory (CNT).

For the molecular species s according to CNT the number of molecules for the smallest stable cluster is given by:

$$j_{*,s} = \left(\frac{8\pi r_{0,s}^2 \sigma_s}{3k_B T \ln S_s^{sat}} \right)^3 \tag{3.16}$$

where $r_{0,s}$ is the molecule radius, σ_s the surface tension of the liquid, k_B the Boltzmann constant, T the gas temperature and S_{sat} the supersaturation ratio given by $S_s^{sat} = p_s/p_s^{sat}$ with p_s the partial pressure of the s molecule species and p_s^{sat} the saturated vapor pressure.

The ratio of formation of primary particles according to [14, 15] is given by:

$$R_s = n_s n_s^{sat} v_s \sqrt{\frac{2\sigma_s}{m_s \pi}} \exp\left(\Theta - \frac{4\Theta^3}{27(\ln S_s^{sat})^2} \right) V_{crit} \tag{3.17}$$

where n_s is the concentration of species s in the gas phase, n_s^{sat} the saturation concentration,v_s and m_s the volume and mass of species s. The normalized surface tension is given by:

$$\Theta = \frac{\sigma_s s_s}{k_B T} \tag{3.18}$$

with s_s the surface area of the molecule.

This approach hold for simple systems of non-reactive species such as Ar/Si or Ar/ZnO. For the **reactive species** nucleation insights from molecular dynamics simulation will be used to tune the CNT in order to define nucleating species and to predict nucleation behavior in e.g. Si/H/N systems, taking into account the effect of Si-H and Si-N monomers, and the effect of the presence in such systems of small quantities of O_2.

In case of species with **extremely low vapor pressure** or more generally of **interatomic potential several orders of magnitude higher then the average thermal energy** of the system, the size of the smallest stable cluster predicted by CNT could be of very few atoms for which the concept of surface tension is not so well defined. Moreover, in the case of very small primary cluster the mesoscopic model scale would be shifted towards the molecular scale, with a substantial increase of the computational effort. For such materials insights from molecular dynamics will be used to check CNT prediction and to provide additional material relations to describe primary particles formation.

In particular, according to the expected computational effort, a minimum mesoscopic model time step can be chosen for each material. Then the average primary particle dimension of the nucleated particles appearing after such time step can be predicted directly from molecular dynamics, substituting the CNT relations equation (3.16) and equation (3.17) with material relations obtained directly from molecular dynamics, parameterized on T and n_s.

3.4.3 Growth

Particle growth occurs by **heterogeneous nucleation** of atoms of the species s from the gas phase. According to [16] the molecules flux towards the surface of the particle in the free-molecular regime $Kn \gg 1$ is given by:

$$F_s = \frac{p_s - p_s^{sat}}{\sqrt{2\pi m_s k_B T^{gas}}} \tag{3.19}$$

while for continuum regime $Kn \ll 1$ is given by:

$$F_s = \frac{D_s(p_s - p_s^{sat})}{r_p k_B T^{gas}} \tag{3.20}$$

For a generic Kn number regime the following interpolation formula may be used:

$$F_s = \frac{D_s}{2r_p}(C_s - C_s^{sat}) \left\{ \frac{1 + Kn}{1 + 1.71Kn + 1.333Kn^2} \right\} \tag{3.21}$$

where D_s is the diffusion coefficient of the condensing species, C_s^{sat} the concentration in equilibrium with the surface, C_s the concentration in the bulk of the volume, and r_p the particle diameter.

3.4.4 Heterogeneous interaction processes

In a reactive system the interaction between solid particles and gas phase atomic and molecular species

can be modelled using different approaches. The kinetic evolution of the system can be described via collision models in which the rate of reaction is accounted for as a probability factor that defines the rate at which the gaseous molecules remain attached to the solid particles after collision. A more complex approach can be used in which chemical reactions are accounted for by using Arrhenius expressions and only the condensation of gas phase species on the surface of solid particles is modelled as a collisional process. Other strategies can be used to model heterogeneous interactions in a $\mathcal{GP}$ reactor, but for the sake of brevity we will fully describe only the second approach presented above. In this case, the interaction between the gas phase species and the solid particles takes place through three distinct processes: **surface reaction**, **condensation** and **hydrogen release**. These are given in [17, 18, 19, 20] and described below for the $\mathcal{GP}$ synthesis of silicon from silanes. Silanes (SiH_4, Si_2H_6, Si_3H_8) react with the particle surface releasing hydrogen, as can be see in table 1, where the surface reactions (S.R.), the deposition phenomena (modelled as a collisional process) of silenes and silylenes on the particles surface (condensation (cond.)), and the hydrogen release (H_2) mechanisms are presented.

Surface reactions

After **surface reaction** with a silane molecule, a primary particle p_x of particle P_q is transformed as

$$\begin{aligned} &P_q(\ldots, p_x(\eta_{\mathrm{Si}}, \eta_{\mathrm{H}}), \ldots, \mathbf{C}) + \mathrm{Si}_i\mathrm{H}_{2i+2} \rightarrow \\ &P_q(\ldots, p_x(\eta_{\mathrm{Si}} + i, \eta_{\mathrm{H}} + 2), \ldots, \mathbf{C}') + i\mathrm{H}_2 \end{aligned} \tag{3.22}$$

Each primary particle is described by the number of silicon atoms η_{Si} and hydrogen atoms η_{H}. $\mathbf{C}$ and $\mathbf{C}'$ are connectivity matrix. $\mathbf{C}'$ is the new connectivity matrix resulting from the addition of surface area. Connectivity matrices are lower diagonal matrices of dimension $n(P_q) \times n(P_q)$, where $n(P_q)$ is the number of primary particles in a particle P_q. The connectivity matrix stores the common surface between two primary particles and describes the sintering between them, as illustrated in [19].

$$\mathbf{C}(P_q) = \begin{pmatrix} 0 & \ldots & 0 & \ldots & 0 \\ C_{21} & \ddots & 0 & \ldots & 0 \\ \vdots & \ddots & \ddots & \ldots & \vdots \\ C_{i1} & \ldots & C_{ij} & \ddots & \vdots \\ \vdots & \ldots & \vdots & \ldots & \vdots \end{pmatrix} \tag{3.23}$$

The element C_{ij} of a matrix $\mathbf{C}$ has the following property

$$C_{ij} = \begin{cases} 0, \\ \text{if } p_i \text{ and } p_j \text{ are non-neighbouring} \\ S_{\mathrm{sph}}(p_i, p_j) \leq C_{ij} \leq s(p_i) + s(p_j), \\ \text{if } p_i \text{ and } p_j \text{ are neighbouring} \end{cases} \tag{3.24}$$

where $S_{\mathrm{sph}}(p_i, p_j)$ and $s(p_i)$, $s(p_j)$ are, respectively, the surface area of a sphere with the same volume of that of primaries p_i and p_j

$$S_{\mathrm{sph}}(p_i, p_j) = \sqrt[3]{\pi}\left[6(\nu(p_i) + \nu(p_j)\right]^{2/3} \tag{3.25}$$

and the primary particle surface for primaries p_i and p_j

$$s(p_i) = \pi(d_{\mathrm{pri}}(p_i))^2 \tag{3.26}$$

The rate of surface reaction is modelled as an Arrhenius process; and is also proportional to the surface area of the particle, S_q, and the gas-phase concentration of silanes [17].

$$R_{\mathrm{SR}} = A_{\mathrm{SR,SiH_{2i+2}}} S_q C_{SiH_{2i+2}} exp\left(-\frac{E_{\mathrm{A,SR}}}{RT}\right) \tag{3.27}$$

where A and E_{A} are the Arrhenius parameters for silane species SiH_{2i+2}. These parameters are given in table table 1.

Condensation

During **condensation** particles grow by the deposition of siagents elicotterolenes and silylenes on the particle surface

reaction	type	A	E_A, kcal/mol
$SiH_4 + p_x \rightarrow p_x(\eta_{Si} + 1, \eta_H + 2) + H_2$	S. R.	3.0×10^{33}	37.5
$SiH_2 + p_x \rightarrow p_x(\eta_{Si} + 1, \eta_H + 2)$	cond.	1.0	-
$Si_2H_6 + p_x \rightarrow p_x(\eta_{Si} + 2, \eta_H + 2) + 2H_2$	S.R.	3.0×10^{34}	37.5
$Si_2H_4A + p_x \rightarrow p_x(\eta_{Si} + 2, \eta_H + 4)$	cond.	1.0	-
$Si_2H_4B + p_x \rightarrow p_x(\eta_{Si} + 2, \eta_H + 4)$	cond.	1.0	-
$Si_3H_8 + p_x \rightarrow p_x(\eta_{Si} + 3, \eta_H + 2)$	S.R.	3.0×10^{34}	37.5
$p_x \rightarrow p_x(\eta_{Si}, \eta_H - 2) + H_2$	H_2	1.2×10^{19}	47.0

Table 1: Heterogeneous interaction processes included in the silicon synthesis mechanism [17].

$$P_q(\ldots, p_x(\eta_{Si}, \eta_H), \ldots, \mathbf{C}) + Si_iH_jX \rightarrow P_q(\ldots, p_x(\eta_{Si} + i, \eta_H + j), \ldots, \mathbf{C}') \tag{3.28}$$

This may be modelled as a collisional process, with rate given by

$$R_{cond} = A_{cond} C_{Si_iH_jX} \sqrt{\frac{\pi k_B T}{2 m_{Si_iH_jX}}} \left(d_{Si_iH_jX} + d_{col,q}\right)^2 \tag{3.29}$$

where A_{cond} is the collisional efficiency of the process (assumed equal to 1.0), $m_{Si_iH_jX}$ and $d_{Si_iH_jX}$ are the mass and diameter of the colliding species, respectively, and $d_{col,q}$ is the collision diameter of particle q [17].

Hydrogen release

The **hydrogen release** from particles is a strong function of temperature and annealing time. The model includes a stochastic jump process to account for release of hydrogen from particles

$$P_q(\ldots, p_x(\eta_{Si}, \eta_H), \ldots, \mathbf{C}) \rightarrow P_q(\ldots, p_x(\eta_{Si}, \eta_H - 2), \ldots, \mathbf{C}') + H_2 \tag{3.30}$$

Assuming that the common surface element remains unchanged due to the loss of hydrogen from the particle surface, the rate of hydrogen desorption is proportional to the coverage (θ_q), which can be calculated as the ratio of number of hydrogen to number of silicon atoms [17]

$$R_{H_2} = A_{H_2} \theta_q exp\left(-\frac{E_{A,H_2}}{RT}\right) \tag{3.31}$$

$$\theta(P_q) = \frac{\sum_{x=1}^{n_q} p_x(\eta_H)}{\sum_{x=1}^{n_q} p_x(\eta_{Si})} \tag{3.32}$$

3.4.5 Bulk composition

An approach used to model the concentration profile within liquid aerosol particles dispersed in a reactive $\mathcal{GP}$ is presented in [21]. A similar approach could be transferred to $\mathcal{GP}$ synthesis of solid particles by modifiying the relevant parameters.

Let a particle be put in an atmosphere containing a reacting gas admixture A. The molecules of A are assumed to react with guest reactant B dissolved in a host material of the particle (in principle, B itself can be the host material). The reactant A is assumed to react with the reactant B along the route

$$A + B \rightarrow C \tag{3.33}$$

The particle initially containing no molecules of A begins to consume those crossing the particle-carrier gas interface. Four stages of the uptake process are considered: diffusion of A toward the particle; crossing the particle air interface; diffusion reaction process inside the particle; and accumulation of non-reacted A molecules in the particle.

Inside the particle, the diffusion-reaction process settles the concentration profile $n_X(r)$

$$\frac{\partial n_X}{\partial t} - D_X \triangle n_X = -k n_A n_B \tag{3.34}$$

$D_X(X$=A, B) is the diffusivity of the reactant molecules inside the particle and in the gas phase,

respectively. k is the binary reaction rate constant for the reaction given by equation equation (3.33).

The boundary condition for the component B corresponds to its zero flux through the interface, that is

$$\left.\frac{\partial n_B}{\partial t}\right|_{r=a} = 0 \tag{3.35}$$

Instead of the boundary condition for A, we use the integral principle

$$\frac{dN_A}{dt} = J_A - k n_A^* n_B^* \int_V f_A(r) f_B(r) d^3r \tag{3.36}$$

where the following notation has been introduced $n_A(r,t) = n_A^*(t) f_A(r,t)$, $n_B(r,t) = n_B^*(t) f_B(r,t)$, $n_B^*(t) = n_B(0,t)$, and

$$N_X(t) = n_X^*(t) Q_X(t) \tag{3.37}$$

where $Q_X(t) = \int_V f_X(r,t) d^3r$. The value $n_X^*(t)$ are the maximum concentrations of the reactants. $f_A(r)$ and $f_B(r)$ are the distribution function of species A and B over coordinates and velocities, and depend on the sticking probability β. If we assume the condensation of A onto a spherical particle

$$f_A^- = (1-\beta) f_A^+ + \frac{\beta}{2\pi} n_{Ae} \tag{3.38}$$

where f^- is the velocity distribution function of molecules flying outword from the particle, f^+ is the same for molecules flying toward the particle surface, and n_{Ae} is the equilibrium concentration of A molecules over the particle surface. The total flux of A is expressed as

$$J_A = \alpha(a)(n_{A\infty} - n_{Ae}) \tag{3.39}$$

Here $n_{A\infty}$ is the concentration of A far away from the particle and $\alpha(a)$ is the condensation efficiency, function of the particle radius a.

3.4.6 Heat transfer and radiation

Heat transfer mechanism in a particle is determined by the ratio between the thermal resistance inside and at the surface of the particle. This ratio is represented by the Biot number:

$$Bi = \frac{\beta_1 h V_p}{k_p S_p} \tag{3.40}$$

with h the heat transfer coefficient, β_1 a Knudsen number accommodation factor from [22], $k_p$the particle thermal conductivity, V_p the volume and S_p the surface of the particle. Under the assumption of spherical particle the ratio $V_p/S_p = R_p/3$.

If $Bi < 0.1$ the temperature inside the particle can be considered as uniform with instantaneous propagation, since the thermal resistance of the surface exceed the thermal resistance of the interior (thermally thin medium). On the contrary, if $Bi > 0.1$ the temperature inside the particle should be considered as spatially and time dependent. An intermediate assumption can be obtained considering uniform interior temperature while maintaining an overall time dependent evolution.

In table 2 the calculated Biot number for different material and gases in plasma reactor conditions assuming Nusselt number $Nu = 2$ and a 100 nm particle diameter is shown ($\beta_1 = 0.55$ for Ar/H_2 and 0.85 for Ar and N_2). Particles can be considered in equilibrium with the gaseous phase for most of the cases considered, with the exception of ZnO particles in a highly conductive environment, such as Ar/H_2 mixtures. Particle with diameter smaller than 100 nm have lower Bi due to high Kn free molecular effects. For this reason in this model we will assume homogeneous interior temperature for particles.

Considering radiation to or from the particle and assuming a zero thermal inertia for particles (no transient), the equilibrium relation for heat transfer is

$$\beta_1 h S_p (T^{gas} - T_p) = \varepsilon \sigma S_p (T_p^4 - T_a^4) \tag{3.41}$$

where T^{gas}, T_p and T_a are the gas, particle and ambient (reactor walls) temperature, ε the emissivity and σ the Stefan-Boltzmann constant. Simple calculations show that for a 100 nm Si particle in Ar gas at 1000 K, and wall temperature at 2000 K, the ratio $(T_{gas} - T_p)/T_p$ is about 0.1%. For this reason in this model the particle radiation is neglected.

		Gas		
		Ar/H_2 65%-35%	N_2	Ar
Material	ZnO	0.143	0.017	0.0083
	Al_2O_3	0.023	0.003	0.0014
	Si	0.003	0.0003	0.0002

Table 2: Biot number for 100 nm nanoparticle of different materials and gases at $3000K$ (plasma reactor conditions).

3.4.7 Reaction energy

Process like surface/bulk reactions (e.g. Si oxidation), nucleation and crystallization release a specific amount of energy directly on the particle surface/or bulk that may lead to an instantaneous increase of the particle temperature with respect to the gas phase. In this model, as a first approximation, we assume that the energy released in such processes is effectively thermostatted or dissipated by the surrounding gas phase, according to the quantitative analysis done in the previous section.

For the oxidization reaction contribution, this assumption especially holds if the oxygen in the system is present only in small quantities as an impurity, which is the case of *NanoDome*.

3.5 Particles dynamics and agglomeration

Interactions between particles occur in the mesoscopic model by means of the interparticle potential and their Brownian driven motion. When particles collides they connect together to form agglomerates of finite size that can contain from 1 to 10,000 particles [5]. The connection of two particles by means of weak forces (e.g. van der Walls) is called **coagulation** and can be broken if another sufficiently energetic collision occurs [23]. As soon as two particle are connected by coagulation they can irreversibly stick together by **sintering**, which is a temperature driven non-reversible process, and may lead in time to complete sintering. Instantaneous sintering between two particles is called **coalescence**. The model and the mathematical implementation of these phenomena are of paramount importance for their correct prediction, as shown in [24, 25, 26, 27, 28].

3.5.1 Interparticle potential

Interaction potential between particles is determined by optimization of a generic U^{MS} mesoscopic potential function using a set of reference atomistic simulations of small representative systems in which a potential function for interatomic potential U^{AT} is used. Iterative Boltzmann inversion [29] or force mapping [30] can be used to define mesoscopic energy functions (interparticle potential) from the atomistic to the coarse grained mesoscopic model in the hypothesis of pairwise potentials.

In the **iterative Boltzmann approach** the objective is finding an optimal U^{MS} given by:

$$U^{MS}(\mathbf{x}) = \sum u^{MS}(r_{ij}) \tag{3.42}$$

where $\mathbf{x}$ and r_{ij} are the spatial arrangement of the particles and the distance between particles in the mesoscopic model. The radial distribution function of the mesoscopic particles $g^{AT}(r)$ is calculated from an atomistic simulation: the mapping matrix is used to define particles position. $g^{AT}(r)$ is used for the evaluation of the $u^{MS}(r)$ pairwise potential between particles. The approximation of radial distribution function for a pair potential in diluite systems $g(r) = \exp(u(r)/k_BT)$, so that:

$$u^{MS}(r) = -k_BT \ln g^{AT}(r) \tag{3.43}$$

Now a mesoscopic simulation is performed using $u^{MS}(r)$ and the radial distribution function $g^{MS}(r)$ is calculated, leading to a correction of $u^{MS}(r)$ given by:

$$u^{MS}_{new}(r) = u^{MS}_{old}(r) - k_BT \ln\left(\frac{g^{AT}(r)}{g^{MS}(r)}\right) \tag{3.44}$$

and iterations are performed until convergence.

The **force matching approach** is based on the definition of a mesoscopic interparticle force as an average of the forces between particles calculated using a representative set of atomistic simulations, so that:

$$\mathbf{F}_i^{MS} = -\frac{\partial U^{MS}(\mathbf{x})}{\partial \mathbf{x}_i} = \left\langle \mathbf{F}_i^{AT} \right\rangle \tag{3.45}$$

which holds for each mesoscopic particle i. The force $\mathbf{F}_{ij}^{MS}(r)$ between two particles is usually approximated as:

$$\mathbf{F}_{ij}^{MS}(r) = -\left(f_{ij}(r) + \frac{1}{4\pi\varepsilon_0}\frac{q_i q_j}{r^2} \right) \frac{\mathbf{r}_{ij}}{r_{ij}} \tag{3.46}$$

where $f_{ij}(r)$ is a spline function, with $\mathbf{r}_{ij} = \mathbf{x}_j - \mathbf{x}_i$.

The optimized form of F_{ij}^{MS} can be found using an objective function to be minimized:

$$\chi = \sum_{k=1}^{n} \sum_{i=1}^{N_{MS}} \left(\mathbf{F}_i^{AT}(\mathbf{x}_k^{AT}) - \mathbf{F}_i^{MS}(\mathbf{x}_k^{AT}) \right)^2 \tag{3.47}$$

where $\mathbf{x}_k^{AT}$ is one of the possible n trajectory configurations of the atomic system.

Such approach has been used in [31] for carbonaceous nanoparticles. C_{60} mesoscopic interparticle potential has been described using $n = 12,000$ sets of atomic configurations for a system of 64 nanoparticles and representing the force field by a spline over a mesh with a grid spacing of approximately 0.0025 nm. The resulting force has been analytically represented as a power expansion $f(r) = \sum_{n=2}^{16} A_n / r^n$.

Both approaches can be used to find the interparticle potential at mesoscopic level. The parameterization will be performed also considering particles size.

Force matching approach will be the preferred method in this model since it does not require mesoscopic model simulations in order to tune the potential. An algorithm for the computation of interparticle potential can be developed for a generic atomistic configuration.

3.5.2 Coagulation

Coagulation occurs when two particles comes in contact as result of their relative motion or due to collision algorithm. While in collision algorithms particle sticking is always assumed to happen, in this model the stability of the connection between the two particles depends only on the interparticle potential $u^{MS}(r)$ and the dynamic of the impact. Sticking occur between two coagulated particles only in case of sintering i.e. in case of a contact time $\tau_C \simeq \tau_S$ where τ_S is the sintering time, so that a rigid structure is formed by means of a neck between the two particles.

In order for coagulation to take place, a connection criterion between two particles p_i and p_j must be defined at each time step in order to check if the interparticle potential $u^{MS}(r)$ can overcome the kinetic energy of the colliding particle system, establishing a stable connection. A simple criterion requiring that $r_{ij} \leq r_0$, where r_{ij} is the interatomic distance between a_i and a_j and r_0 a characteristic connection distance is very easy to implement. Nevertheless it can fail to distinguish between a stable connection and a collision that leave the particles unconnected in case of weak bonding, such as the van der Walls based potentials. In these cases the criterion can be improved adding the requirement that the condition must be satisfied for a time interval $t - t_0$ higher than the characteristic collision time of atoms τ.

A more consistent connection criterion for weak interactions between particles should compare the kinetic energy in the center of mass system and the potential energy of the two particles system, to check if the particles have enough kinetic energy to break the connection. For example, in case of two identical atoms with a pairwise potential (e.g. Lennard-Jones) this criterion can be expressed as

$$\frac{1}{4} m v^2 + u_{ij}^{MS}(r) \leq 0 \tag{3.48}$$

where v is the relative velocity of the two particles, m the reduced mass, r their relative distance and u_{ij}^{MS} the potential energy.

Due to the nature of the potential, coagulated particles can still rotate around each other as shown in 3.3. The rearrangement of rigid clusters by rotation around weakly connected particles has been described in [23].

When two single particles p_i and p_j coagulate, each one representing a single nanoparticle NP_k and NP_l respectively, a new nanoparticle $NP_m = NP_k \cup NP_l$.

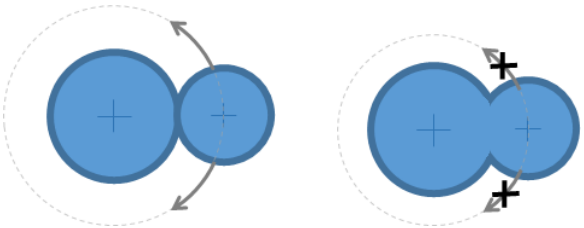

(a) (b)

Figure 3.3: Coagulated (a) and sintered (b) particles.

3.5.3 Sintering

Sintering may occur between two connected (coagulated) particles p_i and p_j. A sketch of a particles pair sintering is shown in figure 3.4. According to [32] the driving force for sintering is a minimization of the free energy resulting in a reduction of surface area. The energy gained by surface reduction is dissipated by viscous flow, which sets the time scale for sintering. The dissipated energy would increase the particle temperature, which in practical processes is effectively thermostatted or dissipated by the surrounding gas.

According to Koch and Friedlander [33] the evolution of the sintering process can be described by

$$\frac{dA}{dt} = -\frac{1}{\tau}(A - A_f) \tag{3.49}$$

where τ is the characteristic fusion time, A the aggregate surface area and A_f the final value upon complete coalescence.

The phenomenological fusion time for two particles can be taken as $\tau = \eta r_{small}/\sigma$ where η is the viscosity, σ the surface tension and r_{small} the radius of the smaller particle in order to take into account sintering of different particle size.

The sintering time τ_S has also been defined by other Authors as

$$\tau_S = \tau_S(p_i, p_j) = A_{sint} d_p \exp(E_{sint}/T) \tag{3.50}$$

where d_p is the minimum diameter of the primary particles p_i and p_j , A_{sint} and E_{sint} are sintering parameters which depend on the particle material.

A detailed theory for multiple particle sintering has been developed in [32] together with different expressions for τ_S depending on the sintering conditions in order to use the simpler Koch and Friedlander model instead of the more complex and computationally expensive method. In particular for sintering of particles in aggregates of N particles the proposed correction to the sintering time is

$$\tau_{S,N} = \tau_S(\frac{N}{2})^{(1/2 - D_f/6)} \tag{3.51}$$

where $\tau_{S,N}$ is the corrected sintering time for a N particle aggregate and D_f the fractal dimension of the aggregate [34].

The sintering parameters can be found in literature or evaluated using molecular dynamics simulations for a representative sets of nanoparticles.

The condition $\tau \to \infty$ (which means a stop in the sintering process) occurs during the condensation process, as soon as d_p increases and T decreases, so that further collisions lead only to "soft agglomerates" formation.

The sintering level between two particles is defined as

$$s(p_i, p_j) = \frac{A_f/A - 2^{-1/3}}{1 - 2^{-1/3}} \tag{3.52}$$

and is comprised between 0 and 1. Tipically a sintering level greater than 0.95 means particles coalescence.

Two coagulated particles are considered partially sintered if the sintering level reaches a threshold level s_{min} that should be defined as input of the model. Particles with $s \geq s_{min}$ become part of an aggregate and behave lake a rigid body with a constraint on the mutual distance that comes from the sintering level of their connection. Particles with $s \leq s_{min}$ are not rigidly connected and behave like a soft agglomerate, with a constraint defined only by their mutual interparticle potential.

Upon complete sintering, when $s \geq 0.95$, particles p_i and p_j are summed together in a single new particle, and the position of the new particle is taken as the position of the bigger one.

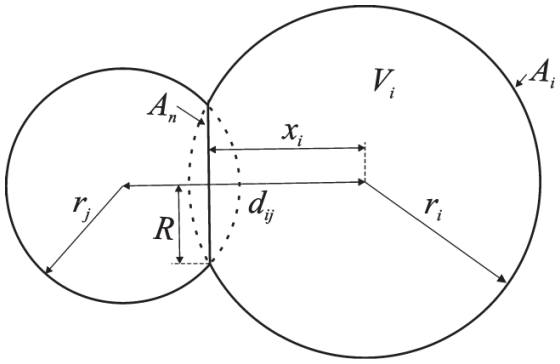

Figure 3.4: Two-dimensional sketch of a pair of spherical particles during sintering [32].

3.5.4 Aggregates

When two particles stick together by sintering then an **aggregate** (hard agglomerate) AG is formed. More particles can then become part of the aggregate by sintering with particles already part of it. Two aggregates can also coagulate to form an agglomerate (soft agglomerate) and the become a single aggregate if sintering occurs between the contact particles.

Interparticle potential between sintered particles has no more effects, while the effects of inteparticle potential between sintered particles and free particles, or particles sintered in another aggregate, are retained.

An aggregate is defined as a structure of sintered particles, evolving in time and whose particles are subject to sintering progress, surface reactions and growth by heterogeneous nucleation.

The **center of mass** of the aggregate can be calculated as

$$\mathbf{x}_{cm}(AG) = \frac{\sum_{i=1}^{N(AG)} m(p_i)\mathbf{x}_i}{m(AG)} \tag{3.53}$$

where $m(AG) = \sum_{i=1}^{N(AG)} m(p_i)$ is the mass of the aggregate and $\mathbf{x}_i$ the particles positions.

The aggreate motion as rigid body is characterized by its center of mass velocity $\mathbf{v}_{CM}(AG)$ and $\omega(AG)$. Velocity of a single particle in the aggregate is

$$\mathbf{v}_i = \mathbf{v}_{CM} + \omega \times (\mathbf{x}_i - \mathbf{x}_{CM}) \tag{3.54}$$

.

The **radius of gyration** for the aggregate is defined as

$$R_G = \sum_i m(p_i) r_i^2 / m(AG) \tag{3.55}$$

where r_i is the distance of the i-th particle from the center of mass of the aggregate.

The **fractal dimension** $D(AG)$ of the aggregate is defined as

$$D(AG) = \frac{\ln(N_r(AG))}{\ln(d_c(AG)/d_{p,av}(AG))} \tag{3.56}$$

where the reduced number of particles in the aggregate is

$$N_r(AG) = \frac{S(AG)^3}{36\pi v(AG)^2} \tag{3.57}$$

the collision diameter is

$$d_c(AG) = 2\sqrt{\frac{5}{3}} R_G \tag{3.58}$$

the average particle diameter is

$$d_{p,av}(AG) = \frac{6v(AG)}{S(AG)} \tag{3.59}$$

and $S(AG)$ and $v(AG)$ are the total area and volume of the aggregate as summation on all aggregate particles.

The moment of inertia of the aggregate can be calculated using the parallel axis theorem as

$$I_{lk} = \sum_{i=1}^{N(AG)} [I_{i,lk}^S + m_i(\sum_j r_{i,j}\delta_{lk} - r_{i,l}r_{i,k})]$$

where $I_{i,lk}^S$ is the moment of inertia of the ith-particle assumed to be spherical.

Upon sticking, the momentum of the particle and aggregate system is preserved, so that $\mathbf{v}_{CM}(AG)$ and $\omega(AG)$ are updated to ensure its conservation.

At each timestep the sintering progress between each particles $p_i, p_j \in AG$ are evaluated according to 3.5.3, so that the interparticle distance d_{ij} is reduced.

The new particles positions can be evaluated by taking the relative distances as constraints and updating all the particle positions, if particles are part of an open chain. If particles are part of a closed chain (cyclic graph) a SHAKE-like algorithm [35] can be used to restructure the overall aggregate shape[36].[3]

In order to reduce the computational cost of such rearrangement it is also possible to neglect the sintering displacement of particles and to rearrange the aggregate shape only when coalescence occurs.

3.5.5 Particles and aggregates motion

Several approaches has been developed in the past [37] to predict the morphology of agglomerates for different Knudsen regimes using particle-cluster and cluster-cluster approaches. The most important algorithms are the Ballistic and Diffusion Limited Agglomeration. These algorithms can be applied both for particle-cluster as in Ballistic Particle Cluster Agglomeration (BPCA) and Diffusion Limited Particle Cluster Agglomeration (DLA), and for cluster-cluster as in Ballistic Cluster Cluster Agglomeration (BCCA) and Diffusion Limited Cluster Cluster Agglomeration (DLCA). These algorithms can be used to determine the typical fractal dimensions of agglomerates that can be used to predict in general their morphology and collisional properties.

In ballistic agglomeration models [39], pairs of clusters (or particles and clusters) are added to each other via linear (ballistic) paths that are selected randomly, without bias, from all possible paths that could result in a "collision" between the two clusters. A typical simulation is started with a large number of particles, and clusters of increasing size are formed as the simulation proceeds [37].

In particle-cluster diffusion limited agglomeration models [40], particles are added one at a time, to a growing cluster of particles via random walk paths that start far outside of the region that is occupied by

[3]While is theoretically possible to impose a constraint on the distance between sintered particles using a fictious sintering potential (to be treated as the interparticle potential), this "rigid" potential would need a smaller timestep than the rest of the system for a stable numerical solution. For this reason a rigid body treatment together with a SHAKE-like approach has been proposed.

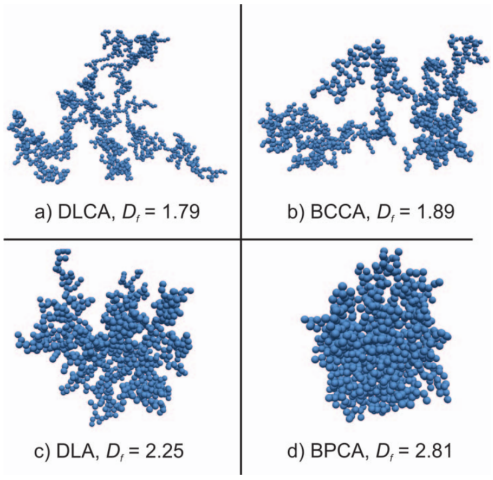

Figure 3.5: Agglomerates consisting of 1024 monodisperse primary particles made by (a) diffusion-limited (DLCA) and (b) ballistic cluster–cluster (BCCA) agglomeration as well as by (c) diffusion-limited (DLA) and (d) ballistic particle–cluster (BPCA) agglomeration [38].

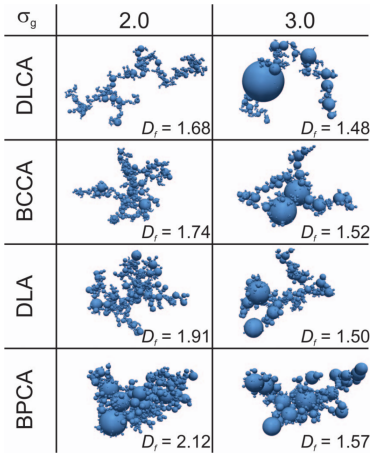

Figure 3.6: Agglomerates of polydisperse primary particles having geometric standard deviation σ g = 2.0 (left column) and 3.0 (right column) made by diffusion-limited (DLCA) and ballistic cluster–cluster agglomeration (BCCA) as well as by diffusion-limited (DLA) and ballistic particle–cluster agglomer- ation (BPCA) [38].

the cluster while in cluster-cluster aggregation model [23] the particles and clusters are moved via random walk trajectories that represent the Brownian motion of particles and aggregates in a dense fluid [37].

The basic version of these algorithms assume that particles stick rigidly together upon contact neglecting sintering. The presence of an interparticle potential that affects the sticking probability can be simulated using the diffusion-limited cluster-cluster aggregation models including a probability that a pair of clusters will join when they come into contact depending on the potential well and kinetic energy of the colliding cluster. This approach is called reaction limited agglomeration.

Results of these different approaches and predicted fractal dimensions of agglomerates are shown in figure 3.5 and figure 3.6.

In this model we want to take into account the possibility of agglomeration depending on a interparticle potential between particles and aggregates. An high level of detail in the description of particles and aggregates motion can be obtained if is assumed to be affected by the gas phase in terms of Brownian motion and calculated using Langevin equation, taking also into account the interparticle potential, as done in [41, 42, 43] for several Kn regimes.

The equation of motion is solve at each time step for each non sintered particle p_i(free or agglomerated) and for each aggregate seen as a rigid body.

The Langevin equation for a **particle** i is written in the form

$$m_i \frac{d^2\mathbf{x}_i}{dt^2} = \mathbf{F}_i(t) - m_i\gamma\mathbf{v}_i + \beta(t) \tag{3.60}$$

with $\langle\beta(t)\rangle = 0$ and $\langle\beta(t)\beta(t')\rangle = 2m_i\gamma k_B T\delta(t-t')$ that represent the stochastic nature of the Brownian motion and $\mathbf{F}_i$ the forces acting on the particle due to interparticle potential. The friction coefficient in continuum regime can be expressed bythe Stokes law as $\gamma = 6\pi\eta R_i$ where η is the viscosity of the gas and R_i the particle radius, while in free molecular regime can be expressed using Epstein relation as

$$\gamma = \frac{4}{3}\delta\pi R_i^2 \frac{p}{k_B T} m_g \langle v_g\rangle \tag{3.61}$$

where δ is a surface accommodation factor which has a value of 1 for specular reflection and a value of 1.444 for diffuse reflection, m_g the gas molecule mass and $\langle v_g\rangle$ the average gas velocity. Transitional regimes has been treated extensively in [43].

The equation for an **aggregate** is the same as equation (3.60) using the gyration radius R_G of the aggregate instead of R_i and the mass of the aggregate. The Brownian force is calculated as the sum of the Brownian forces acting on each particle forming the aggregate; in case of partial sintering the force on a particle is scaled by its effective area. Brownian and interparticle forces are used to define the total force $\mathbf{F}_{tot}$ acting on the center of mass and the torque $\mathbf{T}$ acting on the aggregate as

$$\mathbf{F}_{tot}(AG) = \sum_{i=1}^{N(AG)} (\mathbf{F}_i^{Br} + \mathbf{F}_i) \tag{3.62}$$

$$\mathbf{T}(AG) = \sum_{i=1}^{N(AG)} (\mathbf{x}_i - \mathbf{x}_{CM}(AG)) \times (\mathbf{F}_i^{Br} + \mathbf{F}_i) \tag{3.63}$$

Interparticle potential between sintered particles in not considered, while its effects between sintered particles and free particles, or particles sintered in another aggregate, are retained. The equations of motion for the aggregate are

$$m(AG)\ddot{\mathbf{x}}_{CM}(AG) = \mathbf{F}_{tot}(AG) \tag{3.64}$$

$$\mathbf{I}\dot{\omega} = \mathbf{T}(AG) \tag{3.65}$$

As soon as a new entity became part of the aggregate, establishing a rigid connection by sintering, its linear and angular momentum are preserved and added to the aggregate, influencing its motion. This can have some influence especially in the first stage of aggregate formation, when the aggregate total mass is few time larger than single particles, or in case of aggregation of different aggregates.

The solution of the Langevin equations equation (3.60) and equation (3.64) can be performed using a Verlet-type algorithm as done in [44], while equation (3.65) can be solved using explicit Euler method [45] and then updating the particles positions. A possible approximation consists in neglect-

ing the aggregate rotation (as often assumed in literature).

3.5.6 Possible simplifications in agglomerate formation

The detailed particle and cluster dynamics description described in the previous sections can be potentially very high computationally demanding. For this reason the model will provide a scalable approach in the prediction of agglomerate and aggregate formation, neglecting details in order to reduce the effort and simulation time, while maintaining a state-of-the art description of the cluster formation.

The simplest approach could be implemented neglecting the motion equation and using collision probabilities between nanoparticles to define the rate at which two nanoparticles coagulate (coagulational kernel [46]). In order to do so, we must assume that sticking occurs for each coagulation event and also agglomerates act as rigid bodies. If the equation of motion is not considered then the interparticle potential is neglected. Its effects can still be taken into account as probability of successful sticking upon coagulation, as done in reaction limited algorithms. For each coagulation event two random nanoparticles are selected, randomly rotated and a ballistic collision is then calculated using BCCA algorithms with or without resctructuring [23]. The effect of motion on relative particle position and rotation is then replaced by a stochastic approach. This model is suitable for free molecular flows with $Kn \gtrapprox 1$.

Another approach could be followed, by using DLCA, in which motion of clusters is performed using random walk and not with the solution of an equation of motion. In order to retain the correct time stepping for linking with continuum models, the random walk must be evaluated by taking into account the average displacement due to Langevin dynamics on a cluster of particular fractal dimension, size and mass. Such approach is suitable for diffusion limited regime$Kn \ll 1$.

References

[1] Chiu sen Wang, S.K. Friedlander, and L. Mädler. Nanoparticle aerosol science and technology: an overview. *China Particuology*, 3(5):243 – 254, 2005.

[2] G. Nichols, S. Byard, M.J. Bloxham, J. Botterill, N.J. Dawson, A. Dennis, V. Diart, N.C. North, and J.D. Sherwood. A review of the terms agglomerate and aggregate with a recommendation for nomenclature used in powder and particle characterization. *Journal Of Pharmaceutical Sciences*, 91(10):2013 – 2019, 2002.

[3] W. Gerstner. Crystal form and particle size of organic pigments in printing inks and paints. *J Oil Col Chem Assoc*, 49:954 – 973, 1966.

[4] R.Bandyopadhyaya, A.A. Lall, and S.K. Friedlander. Aerosol dynamics and the synthesis of fine solid particles. *Powder Technology*, 139(3):193 – 199, 2004.

[5] M.L. Eggersdorfer and S.E. Pratsinis. Agglomerates and aggregates of nanoparticles made in the gas phase. *Advanced Powder Technology*, 25(1):71–90, 2014.

[6] M.K. Wu, R.S. Windeler, C.K.R. Steiner, T. Börs, and S.K. Friedlander. Controlled synthesis of nanosized particles by aerosol processes. *Aerosol Science and Technology*, 19(4):527–548, 1993.

[7] K.A. Kusters and S.E. Pratsinis. Strategies for control of ceramic powder synthesis by gas-to-particle conversion. *Powder Technology*, 82:79–91, 1995.

[8] L. Ding, R.L. Davidchack, and J. Pan. A molecular dynamics study of sintering between nanoparticles. *Computational Materials Science*, 45:247–256, 2009.

[9] C. Dopazo and E.E O'Brian. An approach to the autoignition of a turbulent mixture. *Acta Astronaut.*, 1:1239–1266, 1974.

[10] R.L. Curl. Dispersed phase mixing: I. theory and effects in simple reactors. *AIChE Journal*, 9(2):175–181, 1963.

[11] V. Colombo, E. Ghedini, M. Gherardi, P. Sanibondi, and M. Shigeta. A two-dimensional nodal model with turbulent effects for the synthesis of si nano-particles by inductively coupled thermal plasmas. *Plasma Sources Sci. Technol.*, 21:025001, 2012.

[12] S. Shekar, W.J. Menz, A.J. Smith, M. Kraft, and W. Wagner. On a multivariate population balance model to describe the structure and composition of silica nanoparticles. *Computers and Chemical Engineering*, 43:130–147, 2012.

[13] Stephen B. Pope. Gibbs function continuation for the stable computation of chemical equilibrium. *Combustion and Flame*, 139:222–246, 2004.

[14] S.L. Girshick, C.P. Chiu, and P.H. McMurry. Time-dependent aerosol models and homogeneous nucleation rates. *Aerosol Science and Technology*, 13(4):465–477, 1990.

[15] P. Sanibondi. Numerical investigation of the effects of iron oxidation reactions on the fume formation mechanism in arc welding. *J. Phys. D: Appl. Phys.*, 48:345202, 2015.

[16] Sheldon K. Friedlander. *Smoke, Dust and Haze*. Oxford University Press, 1978.

[17] W. J. Menz and M. Kraft. A new model for silicon nanoparticles synthesis. *Combustion and Flame*, 160:947–958, 2013.

[18] William J. Menz, George Brownbridge, and Markus Kraft. Global sensitivity analysis of a model for silicon nanoparticle synthesis. *Journal of Aerosol Science*, 76:188–199, 2014.

[19] William J. Menz, Shraddha Shekar, George Brownbridge, Sebastian Mosbach, Richard Körmer, Wolfgang Peukert, and Markus Kraft. Synthesis of silicon nanoparticles with a narrow size distribution: A theoretical study. *Journal of Aerosol Science*, 44:46–61, 2012.

[20] Weerapong Phadungsukanan, Shraddha Shekar, Raphael Shirley, Markus Sander, Richard H. West, and Markus Kraft. First-principles thermochemistry for silicon species in the decomposition of tetraethoxysilane. *Journal of Physical Chemistry A*, 113:9041–9049, 2009.

[21] Igor Agranovski. *Aerosol: Science and Technology*. Wiley-VCH, 2010.

[22] He-Ping Li and Xi Chen. Three-dimensional modeling of the turbulent plasma jet impinging upon a flat plate and with transverse particle and carrier-gas injection. *Plasma Chemistry and Plasma Processing*, 22(1):27, 2002.

[23] P. Meakin and R. Jullien. The effects of restructuring on the geometry of clusters formed by diffusion-limited, ballistic, and reaction-limited cluster-cluster aggregation. *J. Chem. Phys.*, 89(1):246, 1988.

[24] William J. Menz and Markus Kraft. The suitability of particle models in capturing aggregate structure and polydispersity. *Aerosol Science and Technology*, 47:734–745, 2013.

[25] Markus Sander, Richard H. West, Matthew S. Celnik, and Markus Kraft. A detailed model for the sintering of polydispersed nanoparticle agglomerates. *Aerosol Science and Technology*, 43:978–989, 2009.

[26] William J. Menz, Robert I. A. Patterson, Wolfgang Wagner, and Markus Kraft. Application of stochastic weighted algorithms to a multidimensional silica particle model. *Journal of Computational Physics*, 248:221–234, 2013.

[27] Shraddha Shekar, Markus Sander, Rebecca Shaw, Alastair J. Smith, Andreas Braumann, and Markus Kraft. Modelling the flame synthesis of silica nanoparticles from tetraethoxysilane. *Chemical Engineering Science*, 70:54–66, 2012.

[28] Shraddha Shekar, Alastair J. Smith, William J. Menz, Markus Sander, and Markus Kraft. A multidimensional population balance model to

describe the aerosol synthesis of silica nanoparticles. *ournal of Aerosol Science*, 44:93–98, 2012.

[29] A.P. Lyubartsev and A. Laaksonen. Calculation of effective interaction potentials from radial distribution functions: A reverse monte carlo approach. *Physical Review E*, 52(4):3730, 1995.

[30] S. Izvekov and G.A. Voth. Multiscale coarse graining of liquid-state systems. *J. Chem. Phys.*, 123:134105, 2005.

[31] S. Izvekov, A. Violi, and G.A. Voth. Systematic coarse-graining of nanoparticle interactions in molecular dynamics simulation. *J. Phys. Chem. B*, 109(36):17019, 2005.

[32] M.L. Eggersdorfer, Dirk Kadau, Hans J. Herrmann, and Sotiris E. Pratsinis. Multiparticle sintering dynamics: From fractal-like aggregates to compact structures. *Langmuir*, 27:6358–6367, 2011.

[33] W. Koch and S.W. Friedlander. The effect of particle coalescence on the surface area of a coagulating aerosol. *J. Colloid Interface Sci.*, 140:419–427, 1990.

[34] E. Goudeli, M.L. Eggersdorfer, and S.E. Pratsinis. Aggregate characteristics accounting for the evolving fractal-like structure during coagulation and sintering. *Journal of Aerosol Science*, 89:58–68, 2015.

[35] T.R. Forester and W. Smith. Shake, rattle, and roll: Efficient constraint algorithms for linked rigid bodies. *Journal of Computational Chemistry*, 19(1):102–111, 1998.

[36] M.L. Eggersdorfer and S.E. Pratsinis. Restructuring of aggregates and their primary particle size distribution during sintering. *AIChE Journal*, 59(4):1118–1126, 2013.

[37] P. Meakin. A historical introduction to computer models for fractal aggregates. *Journal of Sol-Gel Science and Technology*, 15:97–117, 1999.

[38] M.L. Eggersdorfer and S.E. Pratsinis. The structure of agglomerates consisting of polydisperse particles. *Aerosol Science and Technology*, 46(3), 2012.

[39] R Jullien. Transparency effects in cluster-cluster aggregation with linear trajectories. *J. Phys. A: Math. Gen.*, 17:L771–L776, 1984.

[40] T.A. Witten and L.M. Sander. Diffusion-limited aggregation, a kinetic critical phenomenon. *Physical Review Letters*, 47(9):1400–1403, 1981.

[41] R.D. Mountain, G.W. Mulholland, and H. Baum. Simulation of aerosol agglomeration in the free molecular and continuum flow regimes. *Journal of Colloid and Interface Science*, 114(1):67–81, 1986.

[42] G .W. Mulholland, R.J. Samson, R.D. Mountain, and M.H. Ernsts. Cluster size distribution for free molecular agglomeration. *Energy & Fuels*, 2:481–486, 1988.

[43] T. Thajudeen, S. Deshmukh, and C.J. Hogan. Langevin simulation of aggregate formation in the transition regime. *Aerosol Science and Technology*, 49:115–125, 2015.

[44] N. Grønbech-Jensen and O. Farago. A simple and effective verlet-type algorithm for simulating langevin dynamics. *Molecular Physics*, 11(8):983–991, 2013.

[45] L. Sanchez Fellay, C. Twist, and M. Vanni. Motion of rigid aggregates under different flow conditions. *Acta Mech*, 224:2225–2248, 2013.

[46] L. Mädler and S.K. Friedlander. Transport of nanoparticles in gases: Overview and recent advances. *Aerosol and Air Quality Research*, 7(3):304–342, 2007.